Key comparison BIPM.RI(I)-K6 of the standards for absorbed dose to water of the LNE–LNHB, France and the BIPM in accelerator photon beams

P. Picard, D. Burns, P. Roger, Franck Delaunay, Jean Gouriou, Maïwenn Le Roy, Aimé Ostrowsky, Line Sommier, Didier Vermesse

Key comparison BIPM.RI(I)-K6 of the standards for absorbed dose to water of the LNE-LNHB, France and the BIPM in accelerator photon beams

S. Picard[1], D. T. Burns[1], P. Roger1, F. Delaunay[2], J. Gouriou[2], M. Le Roy[2], A. Ostrowsky[2], L. Sommier[2], D. Vermesse[2]

[1]Bureau International de Poids et Mesures, Pavillon de Breteuil, F-92312 Sèvres cedex

[2]CEA, LIST, Laboratoire National Henri Becquerel (LNE-LNHB), 91191 Gif-sur- Yvette Cedex, France

ABSTRACT

A comparison of the dosimetry for accelerator photon beams was carried out between the Laboratoire National de Métrologie et d'Essais – Laboratoire National Henri Becquerel (LNE-LNHB) and the Bureau International des Poids et Mesures (BIPM) in March 2012. The comparison was based on the determination of absorbed dose to water for three radiation qualities at the LNE-LNHB. The comparison result, reported as a ratio of the LNE-LNHB and the BIPM evaluations, is 0.995 at 6 MV and 12 MV; 0.994 at 20 MV, with a combined standard uncertainty of 5 parts in 10^3 at all three energies. This result is the fourth in the on-going BIPM.RI(I)-K6 series of comparisons.

1. INTRODUCTION

To compare the absorbed dose to water determinations of the National Metrology Institutes (NMIs) for accelerator photon beams, the Bureau International des Poids et Mesures (BIPM) has developed a transportable standard for absorbed dose to water based on a graphite calorimeter [1, 2]. A comparison programme was adopted in 2008, currently proposed for twelve NMIs, and is registered in the BIPM key comparison database (KCDB) as BIPM.RI(I)-K6 [3]. Within this framework, a comparison has been made between the Laboratoire National de Métrologie et d'Essais – Laboratoire National Henri Becquerel (LNE-LNHB)[1] and the BIPM. The measurements were carried out in the accelerator laboratory of the LNHB in Saclay during the period 5 to 22 March 2012. The BIPM equipment was transported by road.

The comparison between an NMI primary standard and that of the BIPM is established by the reciprocal determination of absorbed dose to water at several accelerator radiation qualities. The BIPM absorbed-dose determination, $D_{w,BIPM}$, is made directly at the NMI using the transportable BIPM standard. The NMI determination, $D_{w,NMI}$, is realized during the comparison using one or more NMI reference ionization chambers calibrated in advance. The comparison result for each quality is the ratio

$$R = \frac{D_{w,NMI}}{D_{w,BIPM}} \qquad (1)$$

and its associated uncertainty $u_c(R)$. A comparison protocol was developed and adopted for guidance before, during and after the comparison [4].

[1] The LNE-LNHB will henceforth be referred to as the « LNHB ».

2. DESCRIPTION OF STANDARDS AND MEASUREMENTS

2.1. The LNHB Determination of Absorbed Dose to Water

The LNHB determination of absorbed dose to water is based on graphite and water calorimetry and the reference absorbed dose to water is the mean of the results obtained using the two methods [5]. The reference point for the D_w determination is at 10 cm depth along the beam axis in a cubic water phantom of side length 30 cm.

Below follows a description of the determination of absorbed dose to water using graphite and water calorimetry, respectively.

1.1.1. Graphite Calorimetry

The LNHB graphite calorimeter (GR9) is used to measure the mean absorbed dose to the graphite of its core, D_{core}, in the LNHB accelerator beams [6]. The ratio between $D_w(V)$ and D_{core} is calculated using the EGSnrc and PENELOPE Monte Carlo codes [7, 8]:

$$D_w = D_{core} \left[\frac{D_w(V)}{D_{core}}\right]_{MC} k_i \, k_{prof}(V) \qquad (2)$$

where MC represents the values obtained by Monte Carlo calculations. The factors k_i and $k_{prof}(V)$ correct, respectively, for the non-graphite material in the core and the difference between calculating $[D_w(V)]_{MC}$ for a volume V rather than for the reference point.

The calibration coefficient $N_{D,w}$ for an ionization chamber can be expressed as

$$N_{D,W} = \frac{D_w}{Q} k_{pol}^{-1} k_s^{-1} k_m^{-1} \qquad (3)$$

where k_{pol}, k_s and k_{rn} are correction factors for polarity, saturation and radial non-uniformity, respectively. The calibration coefficients for the reference chamber NE2571 SN 2791 determined using graphite calorimetry are given in [5].

2.1.1. Water Calorimetry

The LNHB water calorimeter is described in [9, 10]. It contains a quartz vessel, filled with ultra-pure water saturated with nitrogen, and is pre-irradiated before use (≈ 450 Gy). The absorbed dose to water is determined using the equation below:

$$D_w = C_p \, \Delta T \, \frac{1}{1-h} \, k_c \, k_p \, k_\rho \qquad (4)$$

where C_p and ΔT represent the specific heat capacity at constant pressure and the measured temperature increase, respectively. The heat defect is given by h, and for N_2-saturated ultra-pure water it is assumed that $h = 0$. The measurements are corrected for the differences between the measured and the ideal temperature rise (without thermal transfers), taking into account thermal conduction (k_c), the dose perturbation arising from the quartz vessel and the thermal insulation (k_p) and the difference in water density at 4 °C compared to 20 °C (k_ρ). The calibration coefficients for the reference chamber NE2571 SN 2791 determined using water calorimetry, along with other associated information, are given in [5].

2.2. The BIPM Determination of Absorbed Dose to Water

2.2.1. Description of the calorimeter system

The BIPM absorbed-dose graphite calorimeter is described in [1, 2]. No electrical heating is employed, but rather the specific heat capacity of the graphite core, $c_{p,c}$, has been determined previously in a separate experiment [11]. Quasi-adiabatic conditions are achieved by irradiating the core in a graphite jacket that is smaller than the radiation field, resulting in a relatively uniform dose distribution in the jacket. This arrangement is mounted in a PMMA[2] support and vacuum container with graphite build-up plates to centre the core at the reference depth of 10 g cm^{-2}. The mean absorbed dose, D_c, in the graphite core is determined using

$$D_c = c_{p,c}(T) \,.\, \Delta T \,.\, k_{imp} \quad (5)$$

where ΔT is the temperature rise in the core and k_{imp} corrects for non-graphite materials in the core.

Two nominally identical parallel-plate ionization chambers with graphite walls and collector, similar in design to the existing BIPM standards for air kerma and absorbed dose to water, were fabricated for the determination of the absorbed dose to water from the measured absorbed dose to the graphite core. The first chamber is housed in a graphite jacket, nominally identical to the calorimeter jacket, and is irradiated in the same PMMA support and phantom arrangement. The second chamber is mounted in a waterproof sleeve and irradiated with its centre at the reference depth in water. These measurement arrangements are represented schematically in Figure 1.

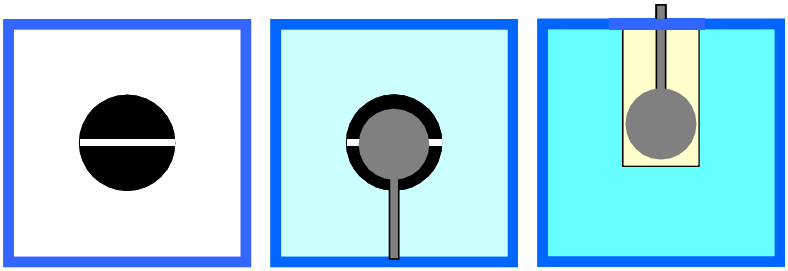

Figure 1. Schematic representation of the three measurement situations. All measurements are made in a cubic PMMA phantom, here represented by the dark blue square. **a)** The calorimeter is used in vacuum and D_c is both measured and calculated. **b)** The graphite core is replaced by the transfer ionization chamber at atmospheric pressure. The ionization charge in graphite, Q_c, is measured and the corresponding cavity dose, $D_{cav,c}$, calculated. **c)** The ionization chamber is placed in a waterproof sleeve inside a similar phantom filled with water. The ionization charge in water, Q_w, is measured and the corresponding cavity dose, $D_{cav,w}$, calculated. The mean absorbed dose to water, D_w, in the absence of the chamber and sleeve is also calculated for a water detector with the same dimensions as the cavity. It follows that a correction factor, k_{rn}, is required for the radial non-uniformity of the radiation field over this dimension, measured for a homogeneous water phantom.

---

[2] Polymethylmethacrylate

The method adopted by the BIPM combining calorimetric and ionometric measurements with Monte Carlo simulations to determine the absorbed dose to water is described in detail in [12] and has previously been applied in [13–15]. The absorbed dose to water D_w is evaluated as

$$D_w = D_c \frac{Q_w}{Q_c} \left(\frac{D_w}{D_c}\right)^{MC} \left(\frac{D_{cav,c}}{D_{cav,w}}\right)^{MC} k_m \qquad (6)$$

where

D_c	- measured absorbed dose to the graphite core;
Q_c	- ionization charge measured when the transfer chamber is positioned in the graphite jacket, replacing the core;
Q_w	- ionization charge measured when the transfer chamber is positioned in water;
$\left(\frac{D_w}{D_c}\right)^{MC}$	- calculated ratio of absorbed dose to water and to the graphite core using Monte Carlo simulations;
$\left(\frac{D_{cav,c}}{D_{cav,w}}\right)^{MC}$	- calculated ratio of cavity doses in graphite and in water using Monte Carlo simulations;
k_m	- measured correction for radial non-uniformity in water.

In abbreviated form, D_w can be expressed as

$$D_w = D_c \frac{Q_w}{Q_c} C_{w,c} k_m \qquad (7)$$

where $C_{w,c}$ represents the total Monte Carlo conversion factor.

2.2.2. Monte Carlo simulations

The Monte Carlo calculations are described in detail in [12] and make use of the PENELOPE code [16][3]. As noted in the preceding section, four geometries are simulated and the accuracy of the method relies on the symmetry of the geometries and the simulation parameters. A novel aspect of this is the use of a disc-shaped transfer chamber whose total graphite thickness on-axis is the same as that of the calorimeter core. Very few of the geometrical bodies appear in only one of the four simulations so that the fine details should not need to be simulated. Nevertheless, a very detailed geometrical model was constructed. Similarly, although detailed electron transport should not be essential for the same reasons, sufficient detail was used to permit the cavity dose to be calculated in a way that gives the same results as a full calculation using event- by-event electron transport (as demonstrated in an earlier work [17]). A notable uncertainty that does not cancel is the ratio of the photon mass energy- absorption coefficients for water and graphite; additional measurements and calculations were made to set an upper limit for this uncertainty. Reference [12] includes a detailed uncertainty analysis for the calculation of the conversion factor $C_{w,c}$.

[3] References [8] and [16] both refer to the PENELOPE code. The authors prefer to clearly ndicate which version has been used for the calculations made by the LNHB and by the BIPM.

The phase-space files of incident photons at 90 cm from the source were supplied to the BIPM by the LNHB, calculated using the EGSnrc and PENELOPE codes [7, 8]. In total, 2.4×10^7 independent photons were supplied, distributed for convenience in 24 files in the format specified in Appendix VI of the comparison protocol [4], which was revised to include particle weights. This is the first comparison in the series for which variance reduction was used in the accelerator simulation. The multiple use of each photon until the statistical uncertainty is optimized is also discussed in the protocol.

The phase-space files are used to calculate $C_{w,c}$ and the corresponding $TPR_{20,10}$. To account for any difference between the calculated $TPR_{20,10}$ and the measured value, the following procedure is adopted. The calculated values for $C_{w,c}$ accumulated so far for the BIPM.RI(I)-K6 comparison series (11 beam qualities in total) are plotted as a function of the corresponding *calculated* $TPR_{20,10}$. A quadratic fit to these data show an r.m.s. deviation within the standard uncertainty of each calculation (typically 0.06 %). Using this quadratic fit, the value for $C_{w,c}$ corresponding to the *measured* $TPR_{20,10}$ is extracted and used for the BIPM determination of absorbed dose in this beam.

The results of the calculations for $C_{w,c}$ are listed in Table 1 along with the measured $TPR_{20,10}$. The figures in parentheses represent the combined standard uncertainty in the trailing digits based on the analysis presented in [12], including components arising from the simulation geometries, input spectra, radiation transport mechanisms and cross-section data used. The statistical standard uncertainty for each value for $C_{w,c}$ extracted from the fit is around 0.04 %.

An additional uncertainty contribution linked to the difference between the measured and calculated values of $TPR_{20,10}$ needs to been taken into account. This uncertainty has been evaluated in terms of its influence on the value of $C_{w,c}$ (cf. Table 7). Interestingly, calculations of the $TPR_{20,10}$ at the LNHB using the same phase-space files agree more closely with the measured values. No explanation has been found for this difference in the $TPR_{20,10}$ values calculated at the BIPM and the LNHB.

Beam quality	**Measured $TPR_{20,10}$**[4]	**Calculated $TPR_{20,10}$**[5]	$C_{w,c}$
6 MV	0.675	0.6688(8)	1.1223(22)
12 MV	0.749	0.7493(7)	1.1345(25)
20 MV	0.783	0.7786(11)	1.1407(27)

Table 1. $TPR_{20,10}$ and conversion factor $C_{w,c}$. The calculated $TPR_{20,10}$ and $C_{w,c}$ for the BIPM calorimeter have been calculated using the phase-space files supplied by the LNHB using the Monte Carlo code PENELOPE [16]. The values in parenthesis represent the combined standard uncertainty based on [12]. Also given are the measured values for the $TPR_{20,10}$ and the values calculated at the BIPM with their statistical standard uncertainty; the combined uncertainties are listed in Table 7.

[4] The measurements giving rise to the $TPR_{20,10}$ are corrected for ion recombination.
[5] The $TPR_{20,10}$ was calculated for a detector of radius 1 cm. Previous calculations at the BIPM used a radius of 2.25 cm.

2.3. Measurements in the High-Energy Photon Irradiation Facilities at the LNHB

2.3.1. The LNHB accelerator used for the comparison

The comparison was carried out using the LNHB accelerator facility, housing a Saturne 43 General Electric linear accelerator[6]. It provides 6 MV, 12 MV and 20 MV photon fields at dose rates ranging from 0.5 Gy/min to 3 Gy/min at the point of maximum dose in water. Rotation of the gantry allows the beam to be delivered at any angle. However, for the present set of measurements the gantry was fixed in the horizontal plane. The source-to-surface distance (SSD) is usually set using a graduated rod and pointer system supplied with the accelerator (in this context, "source" refers to the front of the bremsstrahlung converter). Tungsten collimating jaws are used to define the radiation field. Accelerator stability and beam uniformity checks are performed routinely as part of the quality assurance plan for the accelerator. Variation in the accelerator output over the course of a day is typically 0.1 % as measured by external monitors.

2.3.2. Experimental set up

The comparison measurements were made in the three accelerator photon beams available: 6 MV, 12 MV and 20 MV, whose measured tissue-phantom ratios $TPR_{20,10}$ are given in Table 1. The absorbed dose rate was around 1.7 Gy min^{-1} and the pulse repetition frequency was 200 Hz at 6 MV and 100 Hz at 12 MV and 20 MV.

For the measurements in water, the BIPM cubic PMMA phantom of side length 30 cm was used, positioned at a source-to-surface distance of approximately 90 cm. The field size in the detector plane was 10 cm × 10 cm. The reference point for each ionization chamber was positioned at a distance of 100 cm from the source and at a depth of 10 g cm^{-2} in the BIPM phantom; the density of the 3.81 mm PMMA entrance window was taken into account and a density at 20 °C was assumed for the water.

The ionization chamber readings were normalized to the reference temperature of 20 °C and pressure of 101.325 kPa chosen for the comparison. No correction was made for air humidity; the relative humidity in the accelerator laboratory remained within the interval 20 % to 80 % throughout the comparison. An irradiation time of 60 s was used for all measurements with the calorimeter, the BIPM transfer chambers and the LNHB reference chambers.

The mechanical support normally used at the LNHB was used as a support for the calorimeter phantom and the water phantom in turn (see Figure 2).

2.3.3. Beam monitoring and measurement system

When used with its internal transmission monitor alone, the dose rate from a clinical accelerator is not normally sufficiently stable in time for comparisons of primary standards. For this reason the BIPM used a commercial parallel- plate transmission chamber to serve as a monitor during irradiation (PTW 7862) and a reference class thimble chamber (NE 2571 SN 2106) to determine the stability of the transmission monitor at various times during each day of the comparison. All ionization chamber current measurements are ultimately normalized to the reading of the thimble chamber monitor.

---

[6] Certain commercial equipment, instruments, or materials are identified in this report in order to specify the experimental procedure adequately. Such identification is not intended to imply recommendation or endorsement by the participating institutes, nor is it intended to imply that the materials or equipment identified are necessarily the best available for the purpose.

The transmission and thimble chambers monitors were mounted on a purpose-built PMMA support, fixed to a shadow tray made available by the LNHB (see Figure 3). The support incorporates two temperature probes to measure the temperature close to each chamber. To ensure a similar temperature response, the probe for the thimble chamber is encapsulated in a 'dummy' thimble chamber (seen to the right in the figure). The temperature probe for the monitor chamber is close to the edge of the chamber (not visible in the figure).

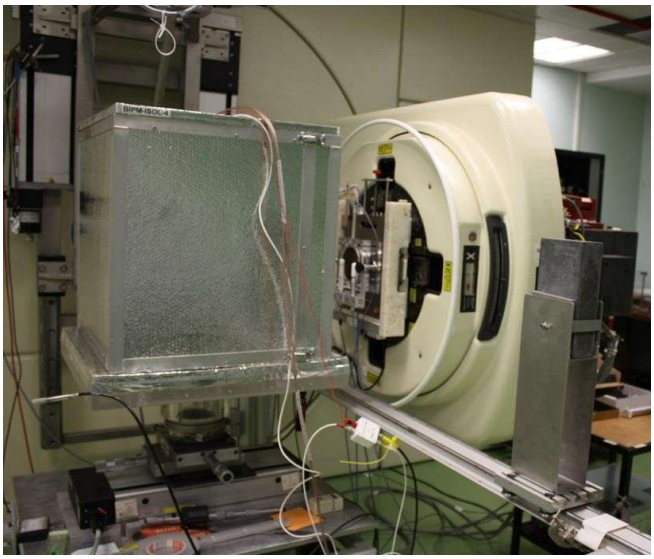

Figure 2. Photograph showing the BIPM calorimeter, inside its insulating protection, mounted in the LNHB accelerator beam. The accelerator head is seen to the right, onto which a metal bar was mounted for use as a reference plane to determine the source- to-surface distance. A sliding lead block (at the right of the photo) mounted on a rail was used for shielding.

Figure 3. The BIPM monitor chamber support in PMMA, fixed on a shadow tray attached to the LNHB accelerator head. The circular transmission chamber is in the centre. The thimble monitor chamber with build-up cap is positioned directly in front of the transmission chamber. A thermistor in a similar cap is positioned to the right of the chamber and measures the temperature under conditions that simulate those of the thimble chamber. The temperature probe for the transmission chamber is placed vertically at the top of the support. A horizontal metal bar can be positioned between the black knobs providing a geometrical reference plane. The thimble chamber is used for long-term beam monitoring and is removed during the actual measurements.

The monitoring procedure was as follows. Before and after each series of measurements made by the BIPM or the LNHB, the thimble chamber monitor, with its POM[7] build-up cap, was positioned on the shadow tray about 1 cm downstream from the external transmission monitor (as shown in Figure 3) and used to calibrate the monitor. In effect, the transmission chamber serves as monitor during each series of measurements while the thimble chamber is used to transfer the monitoring between series of measurements. In this way the uncertainty associated with the monitoring is included in the reproducibility of the repeat measurements for each device, that is, in the statistical standard uncertainties (see Tables 4, 5 and 6).

It follows that it is the thimble chamber that is used to link the BIPM and LNHB dose measurements. That is, over the course of the comparison, this chamber was calibrated using both the BIPM graphite calorimeter and the LNHB transfer standards, which had previously been calibrated against the LNHB graphite and water calorimeters (Section 2.1). The thimble chamber was also used for a robust determination of the charge ratio Q_w/Q_c for the BIPM transfer chambers.

All measurements using an LNHB transfer standard were made using the LNHB measurement system for the standard itself, but exploiting the BIPM monitor system. This system allows the simultaneous measurement of the ionization current or charge, together with the ambient air pressure and the air and water temperatures. For the BIPM transfer chambers, the BIPM data acquisition system was used, air pressure and temperature being measured using the BIPM detectors.

The regular use of the thimble chamber to calibrate the transmission monitor, as well as the need to pre-irradiate all chambers, presents a problem when the BIPM calorimeter is in place because the calorimeter must be shielded during these measurements to avoid unnecessary heating of the core. This was achieved by placing a lead block, 5 cm in thickness, between the calorimeter and the external transmission monitor. However, the block produces backscatter into the external monitor (increasing its response by around 8 %). Therefore, to maintain the symmetry of the measurements and correctly determine the ratio D_c/Q_c, this shielding block was also positioned during the corresponding monitoring for the measurement of Q_c. The block was placed on a sliding carriage supported by a rail that facilitated a reproducible positioning. While some variation in backscatter is unavoidable, its effect will be included in the statistical uncertainty arising from repeated monitoring measurements. In fact, the uncertainty linked to the positioning of the lead block was shown to be negligible.

No lead blocks were used during the monitoring for measurements in the water phantom, that is, for the measurement of Q_w using the BIPM chamber and for the realization of $D_{w,LNHB}$ using the LNHB reference chambers. It follows that, while the final comparison result is independent of the lead backscatter, the measured value for Q_w/Q_c cannot be taken to represent a ratio of cavity doses because it is influenced by backscatter.

---

[7] Polyoxyméthylène, commonly referred to as delrin.

2.3.4. Beam Profile

The BIPM calorimeter core is 45 mm in diameter and, depending on the beam profile, the correction factor for radial non-uniformity k_{rn} can be significant. This is particularly true for clinical accelerators where the uniformity over a 10 cm by 10 cm field can be compromised somewhat so that uniformity specifications are met for all field sizes. The LNHB has measured the beam profile in the horizontal and vertical directions for each beam quality using a thimble chamber. An example for the 12 MV beam is shown in Figure 4. The observed asymmetry of the profile is not unusual for clinical accelerator beams.

The beam profiles measured by the LNHB were used to determine the values for k_{rn} used in this comparison (see equation (6)). A polynomial was fitted to each of the LNHB horizontal and vertical profiles. The correction factor k_{rn} for a given curve is determined by dividing the measured response at the centre by the mean response (weighted by radius) over a diameter of 45 mm. Each value for k_{rn} listed in Table 2 is the mean of the evaluations in the horizontal and vertical directions. The stated standard uncertainty is an estimate based on the difference between the horizontal and vertical scans, as well as on the measurement reproducibility.

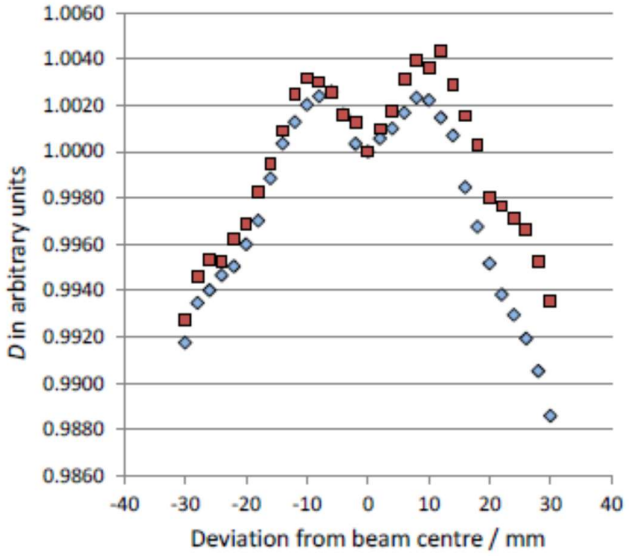

Figure 4. Beam profile measured by the LNHB at 12 MV. The dose D is normalized to the central value. The squares (red) and diamonds (blue) symbols represent measurements in the horizontal and vertical directions, respectively.

Nominal accelerating voltage / MV	k_{rn}
6	1.0056(10)
12	1.0005(15)
20	1.0083(20)

Table 2. Correction factors for radial non-uniformity, k_{rn}, evaluated for a diameter of 45 mm at a depth of 10 g cm^{-2} and for a source-to- detector distance of 100 cm. The uncertainty in the last digits is indicated in parenthesis.

3. RESULTS AND UNCERTAINTIES

In total, fourteen working days were allocated for the comparison. Typically, after setting up a given BIPM device (calorimeter, transfer chamber in graphite or water) and selecting the radiation quality, the monitors were pre-irradiated. Then the BIPM thimble monitor was used to calibrate the transmission monitors, the BIPM device was measured and finally the transmission monitors re-calibrated. Each measurement series normally involved ten measurements. For a given device, the radiation quality was alternated between 6 MV, 12 MV and 20 MV, and repeated two or three times at each quality, before switching to a new device. This entire procedure was repeated for each device to determine the degree of reproducibility. In total, therefore, each device was measured five times for each quality. For calorimetric measurements, the calorimeter was set up on a Friday evening to benefit from the weekend for temperature stabilization and to obtain an adequate vacuum.

3.1. Estimation of Uncertainties

3.1.1. Uncertainty in the determination of $D_{w,LNHB}$

The relative standard uncertainties for the LNHB measurement of the absorbed dose to water using the LNHB primary standards are outlined in Tables 3-a and 3-b, and in Table 3-c. The uncertainties are given for the calibration coefficients determined for an ionization chamber using the LNHB graphite and water calorimeters, respectively. The calibration coefficients listed are not entirely independent. In particular, the correction factors (k_{pol}, k_s, k_{rn}) are the same. The combined uncertainty of the arithmetic mean of $N_{D,w}$ takes into account the correlations. The combined standard uncertainty of the determination of $D_{w,LNHB}$ during the comparison, normalized to the thimble monitor charge Q_{th}, is given in Table 4.

	6 MV	12 MV	20 MV
Relative standard uncertainty components	**$u(y)/y$ / 10^{-3}**		
$[D_w \cdot D_{core}^{-1}]_{MC}$	2.7	2.3	2.6
k_{prof} (MC)	0.8	0.9	1.0
k_i	1.0	1.0	1.0
$D_{core} \cdot Q^{-1}$	1.7	1.7	1.4
k_{pol}	0.4	0.4	0.4
k_s	0.6	0.6	0.6
k_{rn}	0.8	0.8	0.8
Combined relative standard uncertainty $[u_c(y)/y]$ / 10^{-3}:	3.6	3.3	3.4

Table 3-a. Estimated uncertainty contributions for $N_{D,w}$ associated with the determination of absorbed dose to water, $D_{w,LNHB}$, in the 6 MV, 12 MV and 20 MV accelerator photon beams using the LNHB *graphite* calorimeter.

Relative standard uncertainty components	$u(y)/y$ / 10^{-3}
temperature-probe calibration	1.0
temperature-probe positioning	1.0
C_p	1.0
k_c	1.0
k_p	1.0
h	3.0
k_ρ	0.1
ΔT	0.4[8]
Q	1.7
k_{pol}	0.4
k_{s}	0.6
k_{rn}	0.8
Combined relative standard uncertainty $[u_c(y)/y] / 10^{-3}$:	4.3

Table 3-b. Estimated uncertainty contributions for $N_{D,\text{w}}$ associated with the determination of absorbed dose to water, $D_{\text{w,LNHB}}$, in the 6 MV, 12 MV and 20 MV accelerator photon beams using the LNHB *water* calorimeter.

	6 MV	12 MV	20 MV
Relative standard uncertainty components	$u(y)/y$ / 10^{-3}		
$N_{D,\text{w}}$ (graphite calorimeter)	3.6	3.3	3.4
$N_{D,\text{w}}$ (water calorimeter)	4.3	4.3	4.3
k_{pol}	0.4	0.4	0.4
k_{s}	0.6	0.6	0.6
k_{rn}	0.8	0.8	0.8
Combined relative standard uncertainty $[u_c(y)/y] / 10^{-3}$:	2.9	2.8	2.8

Table 3-c. Contributions to the estimated uncertainty of the arithmetic mean of $N_{D,\text{w}}$, associated with the determination of absorbed dose to water, $D_{\text{w,LNHB}}$, in the 6 MV, 12 MV and 20 MV accelerator photon beams. It should be noted that correlation linked to k_{pol}, k_{s} and k_{rn} has been taken into account in the combined relative standard uncertainty.

[8] 0.8×10^{-3} at 6 MV.

	6 MV	12 MV	20 MV
Type A relative standard uncertainty component	**$u_A(y)/y$ / 10^{-3}**		
typical standard deviation of the mean	0.5	0.5	1.0
Type B relative standard uncertainty component	**$u_B(y)/y$ / 10^{-3}**		
$N_{D,w}$	2.9	2.8	2.8
reproducibility	0.7	0.7	0.7
Combined relative standard uncertainty $[u_c(y)/y] / 10^{-3}$:	3.0	2.9	3.1

Table 4. Standard uncertainty components for the determination of $D_{w,LNHB}/Q_{th}$ in the 6 MV, 12 MV and 20 MV accelerator photon beams. The data are derived using the external transmission monitor.

3.1.2. Uncertainties in the determination of $D_{w,BIPM}$

The uncertainties for the determination of D_c, normalized to the thimble monitor charge Q_{th}, are listed in Table 5. The type A standard uncertainty of D_c/Q_{th} depends on the time available for measurements and on the stability of the beam monitoring. The uncertainties associated with the determination of the ratio Q_w/Q_c are listed in Table 6. The chamber orientation corrections noted in Table 6 were determined in the BIPM ^{60}Co reference beam.

	6 MV	**12 MV**	**20 MV**
Type A relative standard uncertainty component	**$u_A(y)/y$ / 10^{-3}**		
typical standard uncertainty of the mean (n = 5)	0.6	1.2	1.0
Type B relative standard deviation component	**$u_B(y)/y$ / 10^{-3}**		
specific heat capacity of graphite [11]	0.9	0.9	0.9
impurity correction	0.2	0.2	0.2
temperature calibration	0.5	0.5	0.5
linear model for temperature extrapolation	0.7	0.7	0.7
axial position of calorimeter	0.5	0.5	0.5
Combined relative standard uncertainty $[u_c(y)/y] / 10^{-3}$**:**	1.5	1.8	1.7

Table 5. Standard uncertainty components for the determination of D_c/Q_{th} at 6 MV, 12 MV and 20 MV. The statistical uncertainty is based on n = 5 determinations for each radiation quality, each one the result of ten irradiations of sixty seconds. The data are derived using the external transmission monitor.

	6 MV and 12 MV	20 MV
Type A relative standard uncertainty component	$u_A(y)/y$ / 10^{-3}	
typical standard uncertainty of the mean (n = 5)	1.1	0.8
Type B relative standard deviation component	$u_B(y)/y$ / 10^{-3}	
difference in graphite jackets of core and transfer chamber	0.1	0.1
chamber orientation for Q_c	0.1	0.1
chamber orientation for Q_w	0.4	0.4
difference in volume for the BIPM transfer chambers	0.3	0.3
temperature and pressure correction	0.3	0.3
axial position of chamber	0.5	0.5
Combined relative standard uncertainty $[u_c(y)/y] / 10^{-3}$:	1.3	1.0

Table 6. Standard uncertainty components for the determination of Q_w/Q_c at 6 MV, 12 MV and 20 MV. The statistical uncertainty is based on n = 5 determinations for each radiation quality, each one the result of ten irradiations of sixty seconds. The data are derived using the external transmission monitor and the thimble monitor.

3.1.3. Combined uncertainty

The significant uncertainties in the determination of $D_{w,LNHB}/Q_{th}$ and $D_{w,BIPM}/Q_{th}$ in high-energy photon beams are listed in Tables 1, 2, 4, 5 and 6. The combined uncertainties for the comparison ratio are listed in Table 7.

	6 MV	12 MV	20 MV
Relative standard uncertainty component	$u(y)/y$ / 10^{-3}		
Calibration of thimble monitor in terms of $D_{w,LNHB}$ (Table 4)	3.0	2.9	3.1
Calibration of thimble monitor in terms of $D_{c,BIPM}$ (Table 5)	1.5	1.8	1.7
Q_w/Q_c for BIPM chambers in LNHB beams (Table 6)	1.3	1.3	1.0
Calculated $C_{w,c}$ for BIPM standard in LNHB beams (Table 1)	2.2	2.5	2.7
$C_{w,c}$ as a function of $TPR_{20,10}$	0.9	0.0	0.7
k_{rn} for BIPM standard in LNHB beams (Table 2)	1.0	1.5	2.0
Combined relative standard uncertainty $[u_c(y)/y] / 10^{-3}$:	4.4	4.7	5.0

Table 7. Standard uncertainty components in the determination of the comparison ratio $D_{w,LNHB}/D_{w,BIPM}$.

3.2. LNHB Realization of D_w during the comparison

The LNHB chose to use two of its reference ionization chambers for the comparison, calibrated in advance. The first, NE2571 SN 2791, was calibrated against the graphite and water calorimeters and the mean calibration coefficient evaluated. The second, NE2577 SN 247/1B, was cross-calibrated against the first. The relevant correction factors and the resulting calibration coefficients are listed in Tables 8-a and 8-b, respectively.

LNHB reference	6 MV	12 MV	20 MV
k_{pol}	0.9991(3)	0.9991(3)	0.9990(3)
k_s	1.0028(6)	1.0055(6)	1.0053(6)
k_{rn}	1.0011(8)	0.9985(8)	1.0048(8)
$N_{D,w}$ / Gy·C^{-1}	4.448×10^7	4.397×10^7	4.334×10^7
$u_c(N_{D,w})$	0.29 %	0.28 %	0.28 %

Table 8-a. Calibration coefficients of the ionization chamber NE2571 SN 2791 for D_w in a 10 cm × 10 cm reference beam. The coefficients are obtained from the mean of the results obtained from graphite and water calorimetry.

LNHB reference	6 MV	12 MV	20 MV
k_{pol}	0.9991(3)	0.9991(3)	0.9990(3)
k_s	1.0028(6)	1.0055(6)	1.0053(6)
k_{rn}	0.9999(8)	0.9994(8)	1.0010(8)
$N_{D,w}$ / Gy·C^{-1}	1.377×10^8	1.360×10^8	1.339×10^8
$u_c(N_{D,w})$	0.34 %	0.33 %	0.33 %

Table 8-b. Calibration coefficients of the ionization chamber NE2577 SN 247/1B for D_w in a 10 × 10 cm reference beam. The coefficients are obtained by a cross calibration against the chamber NE2571 SN 2791.

3.3. BIPM Determination of D_c, Q_w, and Q_c

The BIPM absorbed dose to graphite D_c was obtained by taking the mean of the temperature rise detected by two thermistor bridges (the third bridge was not in operation at the time of the comparison) and applying equation (3) with its correction for impurities, $k_{imp} = 1.0004$.

For practical reasons the BIPM method to convert to absorbed dose to water uses different transfer chambers in water and in graphite. While nominally identical, the two chambers have slightly different volumes and an appropriate correction must be made to the measured charge ratio. Although the air volume for each chamber is determined mechanically during the chamber construction, the values used for the relative volumes are based on ionometric measurements made free in air in the BIPM ^{60}Co reference beam.

The mean values of D_c, Q_c and Q_w, normalized to the thimble monitor charge Q_{th}, are listed for each beam quality in Table 9 along with the statistical standard uncertainties in parentheses. The values for Q_c and Q_w are normalized to the reference air density and corrected for the difference in volume.

Nominal accelerating voltage / MV	D_c/Q_{th} **[Gy μC $^{-1}$]**	Q_c/Q_{th}	Q_w/Q_{th}
6	14.971(9)	3.7044(24)	3.3598(29)
12	18.673(22)	4.6883(16)	4.2478(45)
20	21.252(22)	5.4025(27)	4.9150(28)

Table 9. Experimental results obtained for the BIPM calorimeter and transfer chambers, normalized to the thimble monitor charge, Q_{th}. Values in parentheses represent the statistical standard deviation of the mean.

3.4. Comparison Results

In Table 10 the values determined for $D_{w,BIPM}/Q_{th}$ and $D_{w,LNHB}/Q_{th}$ are given. The values for $D_{w,BIPM}/Q_{th}$ were determined using equation (7) and the relevant values given in Tables 1, 2 and 9 (for convenience, the values for D_c/Q_c, Q_w/Q_{th}, k_{rn} and $C_{w,c}$ are also given in Table 10). The values for $D_{w,LNHB}/Q_{th}$ were determined by making measurements using two reference thimble ionization chambers whose calibration coefficients are given in Tables 8-a and 8-b.

The comparison results are listed in Table 11. The results and the associated standard uncertainties are shown in graphical form as a function of the measured $TPR_{20,10}$ in Figure 5.

Nominal accelerating voltage /MV	D_c/Q_c [Gy μC^{-1}]	Q_w/Q_{th}	k_{rn}	$C_{w,c}$	$D_{w,BIPM}/Q_{th}$ [Gy μC^{-1}]	$D_{w,LNHB}/Q_{th}$ [Gy μC^{-1}]
6	4.041	3.3598	1.0057	1.1223	15.326	15.253
12	3.983	4.2478	1.0005	1.1345	19.203	19.103
20	3.934	4.9150	1.0085	1.1407	22.242	22.104

Table 10. Absorbed dose to water determined by the LNHB, $D_{w,LNHB}$, and the BIPM, $D_{w,BIPM}$. The dose values are given relative to the charge, Q_{th}, measured by the thimble monitor using the external transmission monitor. Also given are the determined values for D_c/Q_c, Q_w/Q_{th} and k_{rn} as well as the total BIPM Monte Carlo conversion factors $C_{w,c}$.

Nominal accelerating voltage / MV	$TPR_{20,10}$	R	$u_c(R)/R$
6	0.675	0.9952	0.0044
12	0.749	0.9948	0.0047
20	0.783	0.9938	0.0050

Table 11. Comparison results for the three radiation qualities, evaluated as the quotient, $R = (D_{w,LNHB}/Q_{th}) / (D_{w,BIPM}/Q_{th})$ and the combined standard uncertainty $u_c(R)/R$.

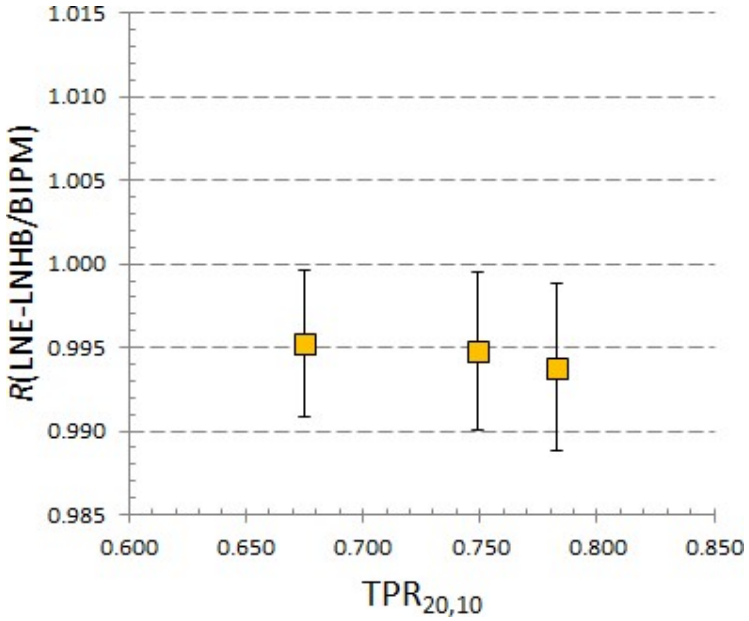

Figure 5. Results of the comparison at high energies of the calorimetric absorbed dose to water standards of the LNHB and the BIPM, shown as a function of $TPR_{20,10}$. The uncertainty bars represent the combined standard uncertainty of each comparison result.

4. DISCUSSION

The LNHB and the BIPM calorimetric standards for absorbed dose to water in accelerator photon beams at 6 MV, 12 MV and 20 MV are in agreement at the level of the standard uncertainty of the comparison of 5 parts in 10^3 at all energies. The measurements were carried out using a horizontal beam. The relative standard deviation of the charge measured by the external transmission chamber over the entire comparison period was around 0.1 % for each beam quality, indicating a relatively high intrinsic stability of the dose delivered over 60 s.

The dimensions of the LNHB transfer chambers are relatively small but the diameter of the BIPM calorimeter core is 45 mm. For this reason, the beam profiles in general give rise to larger correction factors for radial non-uniformity k_{rn} for the BIPM standard compared to those obtained for thimble-type ionization chambers. However, although the mean value obtained from measurements made in two orthogonal directions is close to unity at 12 MV, its uncertainty is estimated at 1.5 parts in 10^3 (cf. Fig. 4). Regarding the limited data available to characterize the non-uniformity in all radial directions at each beam quality and its possible

variation over the duration of the comparison, these standard uncertainties might be under-estimated.

The correction factor for recombination losses in pulsed beams has been determined for the BIPM transfer chambers in a separate series of measurements [19]. While this effect will cancel for the measured ratio Q_c/Q_w, the correction of Q_c for recombination allows the calibration coefficient $N_{D,c}$ measured at different NMIs using the same chamber (calo-3) to be directly compared. This can serve as an additional check on the measurements. The results for the present comparison are consistent with those for previous comparisons with the National Research Council (NRC), Canada [13], the Physikalisch-Technische Bundesanstalt (PTB), Germany [14] and the National Institute of Standards and Technology (NIST), USA [15] at the level of 2 parts in 10^3, which is consistent with the uncertainties.

Monte Carlo calculations of the conversion factor $C_{w,c}$ for different beam qualities have now been made for four comparisons: the NRC, the PTB, the NIST and the LNHB. The results are shown in Figure 6. A quadric fit to the data shows a residual-mean-square deviation of 6 parts in 10^4, which is consistent with the statistical uncertainties.

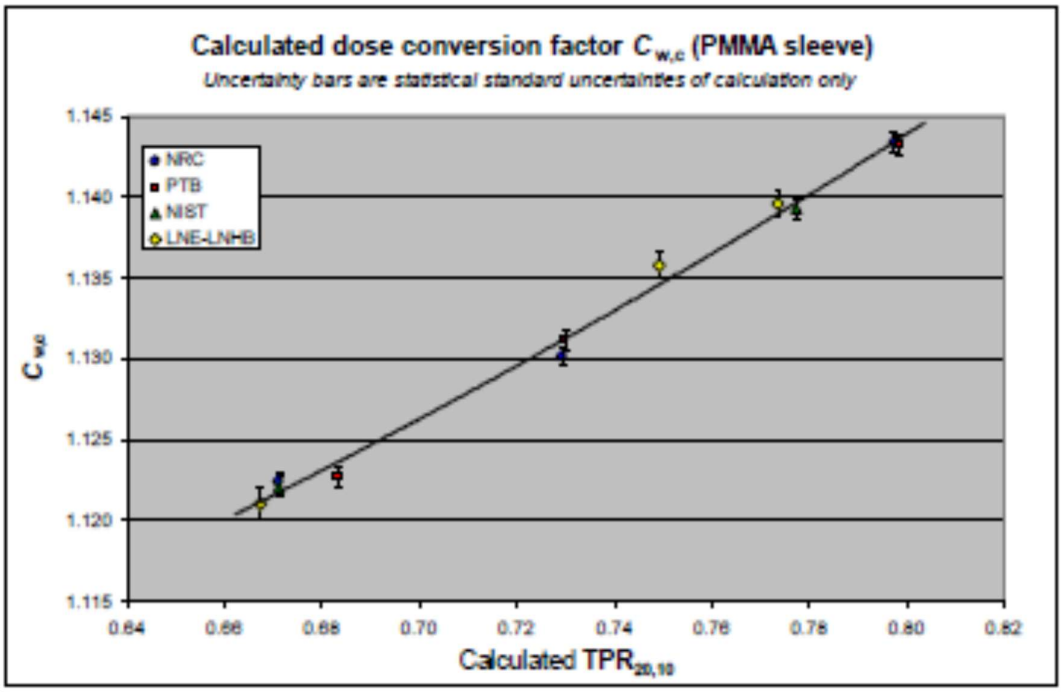

Figure 6. The calculated dose conversion factor $C_{w,c}$ for the BIPM standard, calculated using the phase-space files supplied by the participating NMIs. The line is a quadratic fit to the data, the residual-mean-square deviation about this line being 6 parts in 10^4.

An interesting aspect of these calculations is illustrated by the parameter k_{col}, which involves the cavity doses D_{cav} when the chamber is in water and graphite and the absorbed dose to the collector D_{col} in water and graphite, combined as follows:

$$k_{col} = \left(\frac{D_{cav,w}}{D_{cav,c}}\right)_{MC} \left(\frac{D_{col,w}}{D_{col,c}}\right)^{-1}_{MC} \qquad (8)$$

A linear fit to k_{col} as a function of the calculated $TPR_{20,10}$ shows the values for the NRC, PTB and NIST to be consistent at the level of around 2 parts in 10^4, while k_{col} calculated for the LNHB differs by 2.5 parts in 10^3 at all three beam qualities [20]. No reason has yet been found for this and calculations for $C_{w,c}$ including cavity dose calculations will continue for the ARPANSA and NPL and comparisons.

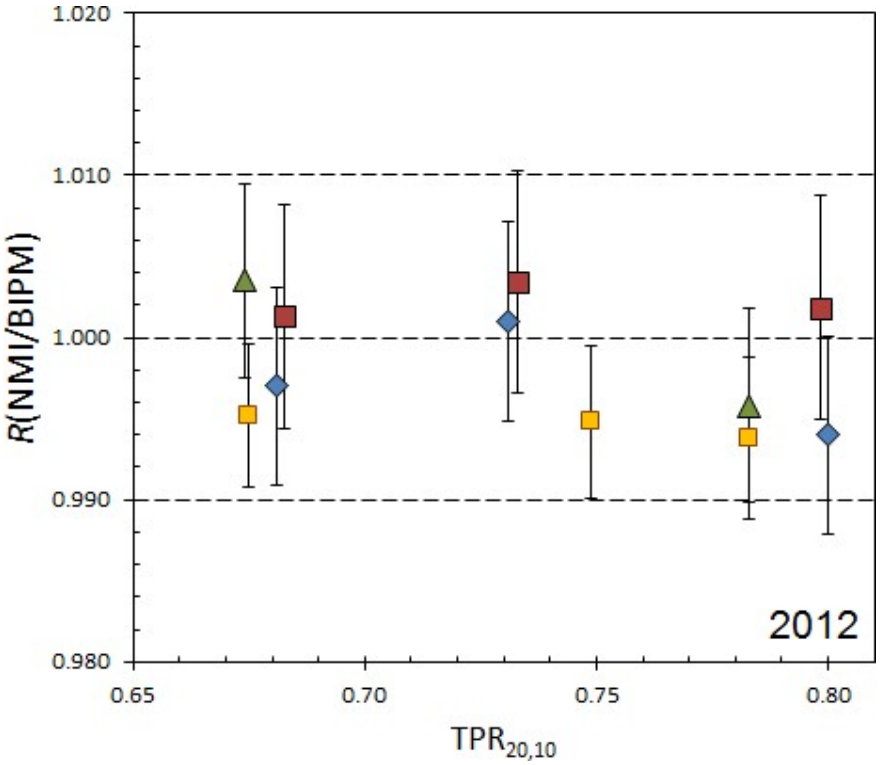

Figure 7. Results of the four comparisons of accelerator dosimetry to date, reported as a ratio of the NMI and the BIPM evaluations of absorbed dose to water for the NRC (blue diamonds) [13], the PTB (red squares) [14], the NIST (green triangles) [15] and the LNHB (yellow squares) as a function of $TPR_{20,10}$. The uncertainty bars represent the standard uncertainty of each comparison result.

Three nominal ranges of radiation qualities are defined for the BIPM.RI(I)-K6 key comparison [3]. The comparison results obtained to date in these three ranges are shown in Figure 7, where comparison data obtained for the NRC [13], the PTB [14], the NIST [15] and the LNHB are indicated. Good agreement between the four NMIs is evident, although it should be noted that the uncertainty bars represent the standard uncertainty of each comparison and are therefore correlated through the common use of the BIPM standard.

5. CONCLUSION

This comparison is the fourth in the on-going BIPM key comparison BIPM.RI(I)- K6. The comparison result, reported as a ratio of the LNE-LNHB and the BIPM evaluations, is 0.995 at 6 MV and 12 MV; 0.994 at 20 MV, with a combined standard uncertainty of 5 parts in 10^3 at all energies.

REFERENCES

[1] Picard S, Burns D T and Roger P 2009 Construction of an Absorbed-Dose Graphite Calorimeter, *Rapport BIPM-2009/01* (Sèvres: Bureau International des Poids et Mesures) 12 pp.

[2] Picard S, Burns D T and Roger P 2010 The BIPM Graphite Calorimeter Standard for Absorbed Dose to Water, abstract to International Symposium on Standards, Applications and Quality Assurance in Medical Radiation Dosimetry *in* Standards, Applications and Quality Assurance in Medical Radiation Dosimetry (IDOS), 2011, vol. 1 55–65, Proceedings Series – International Atomic Energy Agency 2011

[3] Key Comparison BIPM.RI(I)-K6 / BIPM Key Comparison Database http://kcdb.bipm.org/

[4] Calorimetric Comparison of Absorbed Dose to Water at High Energies 2009 BIPM Key Comparison BIPM.RI(I)-K6, *Protocol 1.4– CCRI(I)*[9]

[5] Delaunay F, Rapp B, Daures J, Gouriou J, Le Roy M, Ostrowsky A, Sorel S 2013 New standards of absorbed-dose to water for ^{60}Co and high-energy x-rays at LNE-LNHB : To be published.

[6] Ostrowsky A and Daures J 2008 The construction of the graphite calorimeter GR9 of the LNE-LNHB, CEA-R-6184

[7] Kawrakow I and Rogers D W O 2003 The EGSnrc code system: Monte Carlo simulation of electron and photon transport, Report NRCC PIRS-701, 7 November 2003

[8] Salvat F, Fernandez-Varea J and Sempau J 2003 *PENELOPE*: A code system for Monte Carlo simulation of Electron and Photon transport, *Workshop Proc.* (Issy-les-Moulineaux, France, 7–10 July 2003)

[9] Rapp B, Ostrowsky A and Daures J 2010 Development of a water calorimeter for dosimetry at LNE-LNHB *Revue Française de Métrologie* n° 24 vol. 2010-4 3–8

[10] Rapp B, Ostrowsky A and Daures J 2010 The LNE-LNHB water calorimeter: measurements in a ^{60}Co beam *in* Standards, Applications and Quality Assurance in Medical Radiation Dosimetry (IDOS), 2011, vol. 1 67–74, Proceedings Series – International Atomic
Energy Agency 2011

[11] Picard S, Burns D T and Roger P 2007 Determination of the Specific Heat Capacity of a Graphite Sample Using Absolute and Differential Methods, *Metrologia* **44** 294–302

[12] Burns D T 2011 The dose conversion procedure for the BIPM graphite calorimeter standard for absorbed dose to water, in preparation.

[9] This is the version used for the comparison. An updated version is available on the *KCDB web site*.

[13] Picard S, Burns D T, Roger P, Allisy-Roberts P J, McEwan M, Cojocaru C and Ross C 2010 Comparison of the standards for absorbed dose to water of the NRC and the BIPM for accelerator photon beams, *Metrologia* **47** *Tech. Suppl.* 06025, 22 pp.

[14] Picard S, Burns D T, Roger P, Allisy-Roberts P J, Kapsch R P and Krauss A 2011 Key comparison BIPM.RI(I)-K6 of the standards for absorbed dose to water of the PTB, Germany and the BIPM in accelerator photon beams, *Metrologia **48** Tech. Suppl. 06020*, 21 pp.

[15] Picard S, Burns D T, Roger P, Bateman F B, Tosh R E and Chen- Mayer H 2013 Key comparison BIPM.RI(I)-K6 of the standards for absorbed dose to water of the NIST, USA and the BIPM in accelerator photon beams, *Metrologia* **50** *Tech. Suppl.* 06004, 22 pp.

[16] Salvat F, Fernandez-Varea J M and Sempau J 2009 PENELOPE- 2008: A code system for Monte Carlo simulation of electron and photon transport *NEA No. 6416 Workshop Proc. (Barcelona, Spain 30 June – 3 July 2008)* (Paris: NEA/OECD)

[17] Burns D T 2006 A new approach to the determination of air kerma using primary-standard cavity ionization chambers *Phys*. *Med*. *Biol*. **51** 929–942

[18] Allisy-Roberts P J, Burns D T, Kessler C, Delaunay F and Leroy E 2005 Comparison of the standards for absorbed dose to water of the BNM-LNHB and the BIPM for ^{60}Co γ rays, *Metrologia* **42** *Tech. Suppl.* 06006, 14 pp.

[19] Picard S, Burns D T and Ostrowsky A 2011 Determination of the correction factor for recombination losses of a BIPM ionization chamber of standard design in a pulsed photon beam, *Rapport BIPM-2011/06* (Sèvres: Bureau International des Poids et Mesures) 9 pp.

[20] Burns D T 2013 Status report on Monte Carlo calculations for accelerator dosimetry comparisons *Working document* CCRI(I)/2013- 03 2pp.